Published in final edited form as:

Cancer Res. 2016 April 1; 76(7): 1892–1903. doi:10.1158/0008-5472.CAN-15-2328.

Cystine deprivation triggers programmed necrosis in VHL-deficient renal cell carcinomas

Xiaohu Tang[1,2], **Jianli Wu**[1,2], **Chien-Kuang Ding**[1,2], **Min Lu**[2,3], **Melissa M. Keenan**[1,2], **Chao-Chieh Lin**[1,2], **Chih-An Lin**[1,2], **Charles C. Wang**[1,2], **Daniel George**[3], **David S. Hsu**[2,3], and **Jen-Tsan Chi**[1,2]

[1]Department of Molecular Genetics and Microbiology, Duke University, Durham, North Carolina 27710

[2]Center for Genomic and Computational Biology, Duke University, Durham, North Carolina 27710

[3]Department of Medicine, Duke University, Durham, North Carolina 27710

Abstract

Oncogenic transformation may reprogram tumor metabolism and render cancer cells addicted to extracellular nutrients. Deprivation of these nutrients may therefore represent a therapeutic opportunity, but predicting which nutrients cancer cells become addicted to remains difficult. Here, we performed a nutrigenetic screen to determine the phenotypes of isogenic pairs of clear-cell renal cancer cells (ccRCC), with or without VHL, upon the deprivation of individual amino acids. We found that cystine deprivation triggered rapid programmed necrosis in VHL-deficient cell lines and primary ccRCC tumor cells, but not in VHL-restored counterparts. Blocking cystine uptake significantly delayed xenograft growth of ccRCC. Importantly, cystine deprivation triggered similar metabolic changes regardless of VHL status, suggesting that metabolic responses alone are not sufficient to explain the observed distinct fates of VHL-deficient and restored cells. Instead, we found that increased levels of TNFα (TNF) associated with VHL loss forced VHL-deficient cells to rely on intact RIPK1 to inhibit apoptosis. However, the pre-existing elevation in TNFα expression rendered VHL-deficient cells susceptible to necrosis triggered by cystine deprivation. We further determined that reciprocal amplification of the Src-p38 (MAPK14)-Noxa (PMAIP1) signaling and TNFα-RIP1/3 (RALBP1/RIPK3)-MLKL necrosis pathways potentiated cystine deprived-necrosis. Together, our findings reveal that cystine deprivation in VHL-deficient RCCs presents an attractive therapeutic opportunity that may bypass the apoptosis-evading mechanisms characteristic of drug-resistant tumor cells.

Keywords

Nutrient addiction; Necrosis; Cystine Deprivation; VHL; RIPK1; TNFα; Signaling

Correspondence to: Jen-Tsan Chi.

Conflict of Interest: The authors have declared no conflict of interests for this study.

Introduction

Cellular metabolism comprises various biochemical processes that produce or consume energy and biomolecules by breaking and synthesizing metabolites in the pathways of carbohydrates, fatty acids, and amino acids. Extensive connections exist between metabolism and oncogenic signaling to coordinate the energy status in cancer cells to support their distinct and enormous biosynthetic (macromolecules) and bioenergetic (energy) needs (1-4). While amino acids are building blocks of proteins, different amino acids also provide essential intermediates for various processes: carbon and nitrogen for biosynthesis, the citric acid cycle (TCA) for ATP generation, SAM (S-Adenosyl methionine) for epigenetic modifications, anti-stress capacity to cope with the oxidative stresses. Mammals have at least two major adaptive mechanisms, mTOR (Mammalian TOR (target of Rapamycin)) and GCN2 (general control nonderepressible 2), that sense the amino acids deprivation and trigger amino acid response (AAR) programs. While these adaptive mechanisms often allow for survival, oncogenic events or stresses may render cancer cells "addicted" to certain amino acids and therefore susceptible to death upon their deprivation. Identification of such features in tumors may present therapeutic potential (5). For example, glutamine has been reported to be essential for cancer cells harboring oncogenic events including c-myc activation (6-8), IDH1 (isocitrate dehydrogenase 1) mutation (9) and stresses (10,11). Recently, we and others have found that inflexible tumor metabolic dysregulation in basal-type breast cancer cells exhibit a robust hypoxia program (12). Hypoxia imposed significant metabolic inflexibility and cells death can be affected by nutrient availability (13-15). Leucine deprivation causes extensive apoptotic death in melanoma cells due to absence of autophagy (16).

Although amino acid addictions are becoming appreciated as important metabolic characteristics with therapeutic potential, it is difficult to predict these addictions (5). Therefore, we established a "nutrigenetic screen" by dropping out one (or all) amino acid at a time to determine resulting viability and phenotype of cancer cells with different subtypes or genetic alterations. We identified a profound cystine addiction in *VHL*-deficient clear cell renal cell carcinoma (ccRCC) that was abolished by the restoration of VHL. We also found that the cystine-deprived necrosis involved the activation and reciprocal signaling amplification between the Src-p38-Noxa and tumor necrosis factor alpha (TNFα)-RIPK1/RIPK3-MLKL pathways. While increased TNFα activity in the *VHL*-deficient ccRCC may be essential for tumor progression, this oncogenic predisposition also renders tumor cells susceptible to the cystine-deprived necrosis and provides potential therapeutic opportunities.

Materials and Methods

Materials, tissue culture and amino acid-deprivation protocol

RCC lines (RCC4, 786-O and their VHL-reconstituted counterparts) were provided by Denise Chan (UCSF), which were further authenticated by DDC Medical using short tandem repeat method in Nov 2015. All cells were cultured in DMEM with 10% heat-inactivated FBS, 1% penicillin-streptomycin in a humidified incubator at 37°C and 5% CO_2.

To prepare media deficient in each amino acid, Earle's balanced salt solution was supplemented with 4.5 g/L glucose, 0.37 mM sodium bicarbonate, 24.8 μM ferric nitrates, 10% dialyzed FBS (Sigma) and MEM vitamin solution (Invitrogen). Different amino acid combinations were then added. Cells were plated in the complete DMEM media 1 day prior to PBS-rinsing and amino acid-deprivation.

Cell cytotoxicity and survival

Cell death induced by cystine deprivation, sulfasalazine or erastin was measured by CytoTox-Fluor™ Cytotoxicity Assay (Promega), cell number (crystal violet staining, counting) or CellTiter-Glo® Assay (Promega)). Total caspase activity was determined by Homogeneous caspases assay (Roche). ROS was measured by OxiSelect™ ROS Kit (Cell Biolabs). The Annexin-V/Propidium iodide (PI) assay was performed according to the company protocol (TACS Annexin V – Fluorescein *in situ,* R&D system) using BD FACSCanto II.

Metabolomic profiling

Metabolites were extracted from *VHL*-deficient and *VHL*-reconstituted 786-O exposed to either 200 μM (control) or 1 μM cystine (deprivation) for 18 hours. The metabolite levels in each sample were normalized by Phenol Red (Table S2) and subjected to hierarchical clustering using Cluster 3.0. For specific metabolite associations with genetic events, data were analyzed in GraphPad Prism for correlation and significance.

Western blot analysis

Cells were lysed in RIPA buffer (Sigma) supplemented with protease inhibitor and PhosSTOP phosphatase inhibitor cocktail (Roche). Protein concentrations were determined by BCA protein assay. Equal amounts of protein were loaded for the immunoblot analyses. The signal was detected by the ECL plus Western blotting detection system (Amersham). The detailed procedures were detailed in Supplementary Materials and Methods.

RNA isolation, Affymetrix hybridization and Real-time RT-PCR

RNA was extracted by RNAeasy kit (Qiagen) from RCC cells exposed to control or cystine-deprived media for 6 hours, labeled and hybridized to Affymetrix U133A 2.0 arrays (GSE60422). Total RNA was reverse-transcribed to cDNA using the SuperScript-II reverse transcriptase (Life Technologies) and random hexamers. The level of gene expression was measured by quantitative PCR (qPCR) with Power SYBR Green PCR Mix (Applied Biosystems). All primers were listed in Supplementary Table S5.

Gene expression and signature analyses

Affymetrix probe intensities were normalized by RMA. The changes of gene expression in RCC4 *VHL*-reconstituted cells were derived by zero-transformation ($\Delta\log_2$) against those in control cells. Probe sets that varied by 2 fold in at least 3 samples were selected for hierarchical clustering. We compared the pathway enrichment VHL-null RCC4 (vector) vs. VHL-restored RCC4 (VHL) (GSE60422) using *Gene Set Enrichment Analysis (GSEA)* performed at Broad Public Server using G2 annotated-genesets with default criteria of 1000

permutations (Supplementary Table S1). Similarly, the effects of cystine deprivation on gene expression were derived by zero-transformation and selected probesets that varied by $2^{0.5}$ fold in at least 2 samples (Supplementary Table S3).

Cystine deprivation (CysDep), TNFα and VHL gene signature projection analysis was performed according to (17) and detailed in Supplementary Materials and Methods.

Xenografts drug treatment

1 X 10^6 *VHL*-deficient 786-O cells were implanted subcutaneously into the flanks of NOD.CB17-PrkdcSCID-J mice (The Jackson Laboratory). Tumors were measured 2-3 times per week using a vernier caliper and volumes were calculated using the following formula ($Volume = (width^2 * length)/2$). Once tumor volume reached 200-300 mm^3, animals were randomized into control or treatment group and injected intraperitoneally with PBS (control) or SAS (250 mg/kg; treatment group) once daily for 17 days. Tumor volume was measured twice weekly and reported as ±SD. All experiments were performed following Duke Institutional Animal Care and Use Committee (IACUC) approval in accordance with institutional and national guidelines.

Statistical Analyses

Experimental results were analyzed with a Student's t test using Prism (GraphPad). Data were expressed as mean ± SD with a p value <0.05 was considered statistically significant.

Results

A nutrigenetic screen identified cystine addiction of *VHL*-deficient Renal Cell Carcinoma

To identify nutrient addiction of RCC, we established a “nutrigenetic screen” by dropping out one (or all) amino acid at a time to determine the phenotypic effects. Since the von Hippel-Lindau (VHL) gene is frequently lost or mutated in sporadic ccRCC (18), we selected two isogenic pairs of *VHL*-deficient cell lines, RCC4 and 786-O cells infected by an empty vector (Vec) or wild-type *VHL* for screens. These paired isogenic cells were subjected to the deprivation of each one of 15 amino acids in DMEM (supplemented with dialyzed FBS) to evaluate their effect on viability. As expected, the deprivation of most amino acids arrested proliferation without causing cytotoxicity. One exception was that glycine removal did not inhibit proliferation, similar to our previous findings in MCF7 (19). Interestingly, the deprivation of cystine, the predominant dimeric form of cysteine in media, induced acute and extensive cell death in *VHL*-deficient, but not *VHL*-restored RCC4 and 786-O cells (Fig S1A and S1B). These cells exhibited a swollen morphology, followed by extensive floating debris (Fig S1C). When a cell cytotoxicity assay to quantitate cell death via released protease in media, cystine deprivation triggered massive amounts of released protease in *VHL*-deficient cells, but not *VHL*-reconstituted cells (Fig 1A and S1C). The deprivation of all 15 amino acids (-AA) significantly reduced the cell death caused by cystine deprivation. Next, we exposed the *VHL*-deficient and -restored cells to various cystine levels and found 1.25 μM of cystine triggered cell death in most *VHL*-deficient cells by cell number and crystal violet (Fig 1B, 1C and S1D). In contrast, a similar level of cystine only arrested proliferation in *VHL*-reconstituted cells without significant death.

Cystine is transported into cells by the cystine/glutamate transporter (Xc (-) system) and reduced to cysteine as substrate for the synthesis of glutathione, taurine and other metabolites. To identify the relevant metabolites for cystine-deprived death, we supplemented different metabolites and found that glutathione, but not taurine, protected cells from cystine-deprived death and supported proliferation (Fig 1C). In addition, we found that inhibitors of glutathione synthesis (buthionine sulfoximine (BSO)) or cystine importer xCT (sulfasalazine (SAS)) also triggered extensive death in *VHL*-deficient, but not *VHL*-restored RCC4 (Fig 1D, 1E and S1E). Compared to RCC4 cells, 786-O cells were less sensitive to either BSO or SAS (Fig S1F). However, combining BSO and SAS induced massive cell death in *VHL*-deficient, but not *VHL*-restored 786-O (Fig S1F). We found that primary ccRCC cells, derived from surgically removed RCC tumors without VHL protein expression (Fig S1G), were also extremely sensitive to cystine deprivation or SAS (Fig 1F and 1G). To test the *in vivo* cystine addiction of 786-O xenograft models, we first established the xenografts of 786-O after 4 weeks of subcutaneous injection. After the tumor have established, we treated the mice with SAS and found that SAS treatment significantly reduced tumor growth (Fig 1H, $p = 0.0082$). Together, these data indicated that *VHL*-deficient ccRCC cells and xenografts are profoundly addicted to cystine and sensitive to SAS. In addition, reconstitution of VHL protein expression abolished the cysteine addiction.

Cysteine deprivation induces RIPK1/3-MLKL-dependent necrosis

Next, we investigated the type of cell death in cystine-deprived *VHL*-deficient RCCs. The swollen cell morphology and membrane leakage suggested necrosis instead of apoptosis. We found the cystine-deprived cell death was not associated with PARP1 cleavage, a common marker of apoptosis (Fig 2A). Cysteine deprivation led to a large population of propidium iodide (PI) positive and Annexin-V negative cells (Fig S2A), further suggested a necrotic cell death with loss of membrane integrity. In addition, cystine deprivation reduced, instead of increased, the level of general caspase activity (Fig 2B). Furthermore, a pan-caspase inhibitor Z-Vad-FMK (Z-Vad) failed to protect cystine-deprived death. In contrast, necrostatin-1 (Nec-1), an inhibitor of Receptor-interacting kinase 1 (RIPK1), rescued RCC4 and 786-O cells from cystine-deprived death (Fig 2C and S2B). RIPK1 silencing also rescued cystine-deprived death (Fig 2D). Additionally, we found that Nec-1 also protected the patient-derived primary ccRCC cells from cystine-deprived death (Fig S2C).

Recent investigations of programmed necrosis have identified important roles of RIPK1, RIPK3 (Receptor-interacting kinase 3) and MLKL (Mixed Lineage Kinase domain-Like) (20). MLKL is phosphorylated by RIPK3 and forms oligomers to execute necrosis (21). We observed that Necrosulfonamide (NSA), a MLKL inhibitor, blocked cystine-deprived death in a dose-dependent manner (Fig 2E, 2F and S2D). Cystine deprivation triggered MLKL oligomerization and, to a lesser extent, dimerization and trimerization in both RCC4 and 786-O cells (Fig 2G and S2E). MLKL oligomerizations were verified by two independent phosphor-MLKL antibodies (Fig S2E). NSA also reduced MLKL oligomerization during cystine deprivation in a dose dependent manner (Fig 2G and S2E). However, the MLKL oligomers could not be disrupted into monomers by β-mercaptoethanol (β-ME) or urea, which was different from previous reports (22,23). This may be due to other cystine-deprived modifications, in addition to disulfide bonds, that contribute to the formation of

MLKL aggregates. Furthermore, cystine-deprived MLKL oligomerization was only observed in *VHL*-deficient RCC4 (Fig 2H) and 786-O (Fig S2F) cells but not in *VHL*-reconstituted cells. Collectively, these data clearly indicated that cysteine-deprivation triggered the RIPK1/3-MLKL canonical necrosis pathway, which was suppressed by VHL reconstitution.

VHL prevents cystine-deprived necrosis by suppressing TNFα signaling independent of hypoxia-induced factors (HIFs)

To understand the mechanism by which VHL protected against cystine-deprived necrosis, we performed gene expression analysis on RCC4-Vec and RCC4-VHL cells (GSE60422). The influence of VHL reconstitution on gene expression was derived by a zero transformation (24), in which we compared the transcript level for each gene in *VHL*-restored cells (VHL) to that in *VHL*-deficient cells (Vec). We found that the reconstitution of VHL induced tremendous gene expression changes (Fig 3A). Gene Set Enrichment Analysis (GSEA) indicated that many hypoxia-regulated genes were enriched in *VHL*-deficient cells (Fig 3B and Table S1), consistent with constitutive hypoxia inducible factors associated with *VHL* loss (18). In addition, the target genes of MDM4, EGF and SOX4 were also enriched in the *VHL*-null cells. To examine whether HIFs were involved in cystine-deprived necrosis, we silenced HIF-2α expression in 786-O cells that only expressed HIF-2α without HIF-1α, to avoid potential redundancy among HIFs. While two shRNAs reduced HIF-2α expression in 786-O cells to the level in 786-O *VHL*-restored cells (Fig S3A), they had no protective effects on cystine-deprived necrosis (Fig S3A and S3B). Therefore, the protective effects of VHL were HIFs-independent.

GSEA analysis also identified the enrichment of TNFα pathway in *VHL*-deficient cells (Fig 3B). In agreement with this, we observed higher protein and mRNA expression of TNFα in both *VHL*-deficient RCC4 and 786-O cells (Fig 3C and S3C). A previous report also suggested that VHL repressed the translation of TNFα (25). TNFα can bind TNFα receptors (TNFR) and trigger caspase-8 dependent apoptosis or RIPK1/3-mediated necrosis (26,27). A recent report also indicated that RIPK1 limits caspase-8-dependent, TNFR-induced apoptosis, and animals with RIPK1-knockout exhibit early postnatal lethality mediated by caspase-8 and RIPK3 (28). Interestingly, we observed that silencing of RIPK1 by shRNA in RCC cells caused caspase-8 and PARP1 cleavage (Fig S3D), indicating apoptotic death. The restoration of VHL or silencing of TNFα abrogated the apoptosis induced by silencing of RIPK1 (Fig 3D and 3E). *VHL*-restored cells exhibited increased cleavages of PARP1 and caspase-8 in a confluent culture not related to RIPK1 silencing (Fig S3E). These data supported that increased TNFα activity in *VHL*-deficient cells predisposed them toward apoptosis, which was prevented by the intact RIPK1.

Since RIPK1 blocks increased TNFα-dependent apoptosis in *VHL*-deficient ccRCC, such combination of TNFα-RIPK1 may also render them susceptible to cystine-deprived necrosis. To test this hypothesis, we silenced TNFα in 786-O and RCC4 cells and found a significant reduction in the cystine-deprived necrosis (Fig 3F and S3F) and MLKL oligomerization (Fig S3G). Together, these data indicate that RIPK1 prevents apoptosis caused by the increased TNFα activity in *VHL*-deficient ccRCC. However, high levels of TNFα and intact RIPK1

also predispose *VHL*-deficient RCC to RIPK1-mediated necrosis triggered by cystine deprivation.

Similar metabolomic responses to cystine deprivation in RCC regardless of VHL

Cystine deprivation triggered programmed necrosis in *VHL*-deficient, but not *VHL*-restored RCC cells. One obvious explanation for such life vs. death fate might be their different metabolic response to cystine deprivation. For example, *VHL*-reconstituted cells might consume less and/or able to synthesize more cysteine/GSH from other sources. To investigate such possibilities, we performed metabolomic assays (by Metabolon) in 786-O *VHL*-deficient and *VHL*-restored cells when exposed to regular (HC, 200 μM) or low cystine (LC, 1 μM) for 18 hours (Table S2). We compared the changes of 158 known metabolites under cystine deprivation in *VHL*-deficient and *VHL*-restored 786-O cells. To our surprise, the metabolic responses were largely similar (Fig S4A). Cystine deprivation dramatically reduced cysteine, GSH and GSSG to undetectable levels in both cells (Fig 4A and S4A). Cystine deprivation also increased the levels of sorbitol, acetyl-CoA, asparagine and several metabolites in the γ-glutamyl cycle (Fig S4B). Since intracellular GSH and GSSG were depleted regardless of VHL status, VHL restoration did not prevent cystine-deprived necrosis by maintaining the levels of GSH and GSSG.

Specific induction of Noxa in *VHL*-deficient cells to trigger necrosis

In spite of similar metabolic responses, cystine deprivation increased the level of reactive oxygen species (ROS) in *VHL*-deficient but not VHL-restored cells (Fig 4B). We hypothesized that such distinct changes in ROS may be caused by different transcriptional response to cystine deprivation. Therefore, we performed gene expression analysis to compare the transcriptional responses to cystine deprivation (GSE60422). Zero-transformation identified shared and distinct transcriptional responses between the *VHL*-restored and *VHL*-deficient RCC (Fig 4C and Table S3). For example, GADD45A/B, CTH, XBP1 and SLC7A11 were induced in both cells (Fig 4C and 4D). SLC7A11 encodes an xCT subunit responsible for cystine uptake. Therefore, its induction may reflect the cells' adaptive response to import more cystine during cystine deprivation. The transcriptional responses seen only in VHL-deficient cells included the induction of IL8, ANGPLT4 and PLAU (Fig 4C) as well as ATF3 and Noxa (Fig 4C and 4D). We confirmed the induction of Noxa protein by cystine deprivation (Fig 4E). Noxa is a pro-apoptotic protein that targets mitochondria to induce apoptosis (29). Therefore, we were interested in whether this apoptotic protein also participated in cystine-deprived necrosis. The silencing of Noxa by two shRNAs significantly reduced death in 786-O and RCC4 cells (Fig 4F and S4D). Taken together, these results demonstrated that the specific induction of the pro-apoptotic Noxa in *VHL*-deficient ccRCC contribute to the cystine-deprived necrosis.

The Src-p38 signaling pathway is required for cystine-deprived necrosis

In response to some apoptotic stimuli, reactive oxygen species (ROS) induce Noxa expression via MAPK signaling pathways (30). To identify the specific MAPK responsible for cystine-deprived necrosis, we tested a set of inhibitors of MAPKs or oxidases. We found that the inhibitors of JNK (SP600125), PI3K (LY294002) and NADPH oxidase (VAS-2870) did not affect cystine-deprived necrosis (Fig S5A). In contrast, the p38 MAPK inhibitor

SB203580 protected both RCC4 and 786-O cells from cystine-deprived necrosis (Fig 5A, S5A and S5B). Furthermore, cystine deprivation increased p38 phosphorylation and the p38 inhibitor abolished induction of Noxa (Fig 5B). Consistent with their protection from cystine-deprived necrosis, Nec-1 treatment and VHL reconstitution also attenuated increased p38 phosphorylation and Noxa induction (Fig 5B, 4E and S5C). These data suggested that such signaling differences may account for the distinct life vs. death fate upon cystine deprivation.

The tyrosine kinases Src and FAK can be activated by either ROS or TNFα and play critical roles in cellular signal transduction pathways including p38 (31). We examined effects of the Src inhibitor (Su6656) and FAK inhibitor (PF-573228) on cystine-deprived necrosis. We found that Su6656, but not PF-573228, protected both RCC cells from cystine-deprived necrosis (Fig 5C and S5D). Furthermore, Src silencing protected cells from cystine-deprived necrosis (Fig 5D and S5E). These results indicated that Src was a critical component for cystine-deprived necrosis.

Next, we fractionated cells to examine protein translocations between different sub-cellular components during cystine deprivation. Cystine deprivation increased RIPK1 protein in the heavy membrane fraction (Triton-insoluble fraction after centrifugation at 15,000 x g) (Fig 5E, right panel) of *VHL*-deficient cells, similar to what was reported in TNFα induced necrosis (32). In contrast, cystine deprivation did not increase the RIPK3 or Caspae-8 in the membrane fraction, but reduced their levels in the cytosolic fraction of *VHL*-deficient cells (Fig 5E). Interestingly, we found that cystine deprivation triggered Src modification(s) that significantly slowed its migration pattern into smear (Fig 5E). Since Src is a membrane-anchored protein, such Src smears were prominent in the triton-insoluble membrane fraction of *VHL*-deficient cells, but not *VHL*-restored cells. This modified Src was accompanied by the translocation of RIPK1 protein, further suggesting an important role. However, the nature of Src modifications upon cystine deprivation remained unclear. We ruled out several protein modifications, including K48- and K63-ubiquitination, sumoylation and (carboxymethyl)lysine (*CML*) modification (Fig S5F). Together, these results indicated that cystine deprivation in *VHL*-deficient ccRCC activates the Src-p38 signaling pathway, which contributed to cystine-deprived necrosis. During this process, the Src protein becomes modified by unknown modifications that change its migration pattern.

Reciprocal amplification of the Src-p38-Noxa triggering pathway and TNF-RIP1/3-MLKL necrosis pathway propagates cystine-deprived necrosis

While apoptotic Noxa and necrotic MLKL protein are two distinct effectors of different signaling pathways, both proteins target mitochondria and lead to mitochondria permeabilization (21,33). Mitochondria complex I and III of the electron-transport chain are a major source of cellular ROS (34), which could act to amplify the signal during cystine deprivation. We found that the complex I inhibitor, rotenone, strongly protected RCC4 (Fig 6A) and 786-O (Fig S6A and S6B) from cystine-deprived death. Necrox-5 (Nec-5), a mitochondria ROS scavenger (35), also protected cells death under cystine deprivation (Fig 6B and S6B). As expected, rotenone and Nec-5 strongly abolished Noxa induction and attenuated p38 phosphorylation under cystine deprivation, similar to the Src inhibitor

Su-6656 (Fig 6C). These results implicated the mitochondrial ROS signaling in amplification of the cystine-deprived necrosis.

Similarly, we observed that suppression of Noxa induction also significantly attenuated its upstream kinase p38's phosphorylation (Fig 6D and S6C). Accordingly, suppression of TNFα-RIP1/3-MLKL pathway by TNFα silencing or Nec-1 also reduced both p38 phosphorylation and Noxa induction during cystine deprivation (Fig 6E). These results suggested that inhibition of either component in the necrosis signaling could limit activation of upstream or downstream components. Collectively, these data suggested that mitochondrial ROS generation was critical in the amplification loop of necrosis during cystine deprivation. While cystine deprivation initiates the signaling cascade, the two downstream mitochondria-targeting effectors, Noxa and MLKL, are required to generate a reciprocal amplification loop between the Src-p38-Noxa and TNF-RIP1/3-MLKL necrosis pathways that ultimately results in necrosis.

Enrichment of cystine-deprivation and TNFα gene signatures in *VHL* negative ccRCC

As shown above, the TNFα signaling pathway was required for cystine-deprived necrosis. We projected a defined TNFα gene signature (TNFα-Sig (36), Table S4) to the gene expression profile of RCC4 cells and found higher activity of TNFα-Sig in *VHL*-deficient cells (Fig S6D), consistent with a higher level of TNFα signaling in these cells analyzed by GSEA (Fig 3B). In addition, we defined 115 probesets altered by cystine deprivation as the cystine-deprived gene signature (CysDep-Sig, Fig 4C and Table S3), performed signature projection analysis and found higher activity of CysDep-Sig in *VHL*-deficient cells (Fig S6E). We then performed CysDep-sig and TNFα-Sig projection analysis on the dataset of ccRCC tumors and their paired normal tissues (GSE36895) (37). Consistent with our observations in cell lines, the pathway activities of both TNFα-Sig (Fig 6F and S6F) and CysDep-Sig (Fig 6G and S6G) were significantly higher in the ccRCC tumor samples that associated with lost/mutated VHL. While CysDep-Sig and TNFα-Sig included ~100 probesets respectively, but only 4 probesets overlapping, the activities of CysDep-Sig and TNFα-Sig were highly correlated in tumor dataset ($p<0.0001$, Fig 6H). Similarly, a similar strong correlation between CysDep-Sig and TNFα-Sig pathway was found in 606 RCC tumor dataset from TCGA. Both activities of CysDep and TNFα also negatively correlated with activity of VHL in tumors (Fig S6H). Such high correlation suggested that cystine addiction might be associated with increased TNFα activity and a common feature of *VHL*-deficient ccRCC cell lines or tumors as a predictor of cystine addiction.

Low doses of erastin trigger programmed necrosis as cystine deprivation in RCC cells through RIPK1

Erastin, originally identified to target oncogenic-mutated Ras cells through mitochondrial voltage-dependent anion channels (VDACs) (38), is recently shown to inhibit xCT and induce ferroptosis: an iron-dependent form of non-apoptotic cell death (39). We examined the sensitivity of the isogenic pairs of *VHL* deficient and restored ccRCC cells to erastin. We found that low doses (1-2 μM) erastin induced extensive cell death with protease release in *VHL*-deficient RCC4 and 786-O cells, but not *VHL*-restored cells (Fig 7A and S7A). VHL restoration offered less protection to high dose of erastin (5 or 10 μM) (Fig S7A). In

addition, low doses of erastin also induced Noxa protein in *VHL*-deficient, but not in *VHL*-restored ccRCC cells, similar to cystine deprivation (Fig 7B and S7B). Therefore, we examined whether low doses of erastin utilize the same signaling pathways to induce canonical necrosis as cystine deprivation. Indeed, the silencing RIPK1, TNFα or Noxa all rescued erastin-induced death (Fig 7C S7A and S7C). Taken together, these results suggested that low doses of erastin trigger canonical necrosis in *VHL*-deficient ccRCC via a similar mechanism with cystine deprivation.

Collectively, our data allow us to propose a novel model of cystine-addiction in *VHL*-deficient ccRCC (Fig 7D). While the increased TNFα signaling associated with VHL loss contributes to tumor progression, such a pre-existing architecture required RIPK1 or the necrosome complex to inhibit caspase-8 mediated apoptosis. The delicate balance between TNFα and RIPK1 was extremely sensitive to redox level regulated by cystine-derived GSH, and caused tumor cells to be vulnerable to cystine deprivation or inhibition of cystine transport. Therefore, cystine addiction may present a novel form of nutrient addiction that co-opts the pre-existing oncogenic signaling pathways as potential promising therapeutic approach.

Discussion

While cysteine is appreciated as a limiting component of GSH synthesis that can be therapeutically targeted, much remains unknown about the susceptible tumor types and underlying mechanisms. Here, we have uncovered a specific cystine addiction in *VHL*-deficient ccRCC that is based on the pre-existing signaling changes associated with VHL loss. Since cystine deprivation depletes intracellular GSH in both cystine-addicted and -independent cells, metabolic differences cannot readily explain the dramatic differences of necrosis vs. live. In the cystine-addicted cells, increasing TNFα associated with *VHL* loss requires RIPK1 to prevent apoptosis. However, these increased activities of TNFα and RIPK1 in *VHL*-deficient cells render them vulnerable to cystine-deprived necrosis that is propagated by mutual amplification between the Srcp38-Noxa and TNFα-RIPK1/RIPK3-MLKL pathways. While in cystine-independent cells, low activities of TNFα and RIPK1 renders cells insensitive to cystine-deprivation.

Although the regulation of HIFs protein stability is the most recognizable activity of VHL, VHL also has HIFs-independent actions. Now, others (25) and we showed that VHL suppresses the TNFα signaling in a HIF-independent manner. TNFα gene signatures are also enriched in ccRCC, whose VHL is often lost or mutated. Higher levels of TNFα in tumors often contribute to tumor proliferation, migration, invasion and angiogenesis (40,41). These increased TNFα pathways may also bring about a vulnerability that can be therapeutically exploited, such as the necrosis triggered by either cystine deprivation or xCT inhibitors. Cystine addicted cells may rely on continuous cystine import and *de novo* GSH synthesis to protect from higher levels of oxidative stress. Therefore, such convergence of cystine addiction and tumor progression may open a significant therapeutic window for clinical benefit.

Erastin was first discovered based on its ability to selectively eradicate tumors with oncogenic Ras mutations (38). Further studies have implicated the ability of erastin to block xCT and cystine transport in a form of iron-dependent death called ferroptosis (39). In these studies, glutathione peroxidase 4 (GPX4) and lipid oxidation, but not components of necrosis (RIPK1, RIPk3 and MLKL), involved in ferroptosis (42). However, our data suggested that low dose of erastin shares a similar necrosis death mechanism as cystine deprivation since the silencing of RIPK1, TNFα and Noxa all rendered RCC resistant to low doses of erastin. In previous studies, RIPK1 silencing was not able to prevent cell death under higher doses of erastin. These inconsistencies can be caused by different doses of erastin (low vs. high) or different genetic contexts of the cell types (wide type renal tubule vs. *VHL*-deficient RCC).

Our findings of the cell-type specific cystine addiction associated with VHL loss may present therapeutic opportunities to target these clinically challenging tumors (43,44). While sulfasalazine has been shown to reduce tumor growth and distant metastases in xenograft models of head/neck and breast cancer (14,45,46), our studies provide additional novel insights. First, cystine addiction is found only in a *VHL*-deficient ccRCC with a significant therapeutic window. Second, since cystine deprivation triggers necrosis instead of apoptosis, it may bypass many chemo-resistant mechanisms that generally avoid apoptotic pathways. Sunitinib is a FDA approved drug for ccRCC, which has significant cytotoxic effects (47). However, RCC has been reported to resist this drug treatment (48) that present clinical challenges. Cystine deprivation may bypass these apoptosis-evading mechanisms and trigger necrosis. Last, high GSH levels are usually associated with chemoresistance (49). Therefore, cystine deprivation may deplete intracellular GSH and overcome chemoresistance. For clinical translation, it will be important to further elucidate intrinsic addiction mechanisms and define predictive biomarkers to identify patient populations sensitive to cystine-targeted therapies.

Supplementary Material

Refer to Web version on PubMed Central for supplementary material.

Acknowledgments

We are grateful to members of Chi lab for critical discussions and editing of the manuscript.

References

1. Lunt SY, Vander Heiden MG. Aerobic glycolysis: meeting the metabolic requirements of cell proliferation. Annual review of cell and developmental biology. 2011; 27:441–64.
2. Dang L, White DW, Gross S, Bennett BD, Bittinger MA, Driggers EM, et al. Cancer-associated IDH1 mutations produce 2-hydroxyglutarate. Nature. 2009; 462(7274):739–44. [PubMed: 19935646]
3. Sreekumar A, Poisson LM, Rajendiran TM, Khan AP, Cao Q, Yu J, et al. Metabolomic profiles delineate potential role for sarcosine in prostate cancer progression. Nature. 2009; 457(7231):910–4. [PubMed: 19212411]
4. Tang X, Lin CC, Spasojevic I, Iversen E, Chi JT, Marks JR. A joint analysis of metabolomics and genetics of breast cancer. Breast Cancer Res. 2014; 16(4):415. [PubMed: 25091696]

5. Keenan MM, Chi JT. Alternative fuels for cancer cells. Cancer journal. 2015; 21(2):49–55.
6. Yuneva M, Zamboni N, Oefner P, Sachidanandam R, Lazebnik Y. Deficiency in glutamine but not glucose induces MYC-dependent apoptosis in human cells. J Cell Biol. 2007; 178(1):93–105. [PubMed: 17606868]
7. Wise DR, DeBerardinis RJ, Mancuso A, Sayed N, Zhang XY, Pfeiffer HK, et al. Myc regulates a transcriptional program that stimulates mitochondrial glutaminolysis and leads to glutamine addiction. Proc Natl Acad Sci U S A. 2008; 105(48):18782–7. [PubMed: 19033189]
8. Gao P, Tchernyshyov I, Chang TC, Lee YS, Kita K, Ochi T, et al. c-Myc suppression of miR-23a/b enhances mitochondrial glutaminase expression and glutamine metabolism. Nature. 2009; 458(7239):762–5. [PubMed: 19219026]
9. Bosveld F, Rana A, Lemstra W, Kampinga HH, Sibon OC. Drosophila phosphopantothenoylcysteine synthetase is required for tissue morphogenesis during oogenesis. BMC Res Notes. 2008; 1:75. [PubMed: 18759961]
10. Lamonte G, Tang X, Chen JL, Wu J, Ding CK, Keenan MM, et al. Acidosis induces reprogramming of cellular metabolism to mitigate oxidative stress. Cancer Metab. 2013; 1(1):23. [PubMed: 24359630]
11. Metallo CM, Gameiro PA, Bell EL, Mattaini KR, Yang J, Hiller K, et al. Reductive glutamine metabolism by IDH1 mediates lipogenesis under hypoxia. Nature. 2012; 481(7381):380–4. [PubMed: 22101433]
12. Gatza ML, Kung HN, Blackwell KL, Dewhirst MW, Marks JR, Chi JT. Analysis of tumor environmental response and oncogenic pathway activation identifies distinct basal and luminal features in HER2-related breast tumor subtypes. Breast Cancer Research. 2011; 13(3):R62. [PubMed: 21672245]
13. Kung HN, Marks JR, Chi JT. Glutamine synthetase is a genetic determinant of cell type-specific glutamine independence in breast epithelia. PLoS genetics. 2011; 7(8):e1002229. [PubMed: 21852960]
14. Timmerman LA, Holton T, Yuneva M, Louie RJ, Padro M, Daemen A, et al. Glutamine Sensitivity Analysis Identifies the xCT Antiporter as a Common Triple-Negative Breast Tumor Therapeutic Target. Cancer Cell. 2013
15. Keenan MM, Liu B, Tang X, Wu J, Cyr D, Stevens RD, et al. ACLY and ACC1 Regulate Hypoxia-Induced Apoptosis by Modulating ETV4 via alpha-ketoglutarate. PLoS Genet. 2015; 11(10):e1005599. [PubMed: 26452058]
16. Sheen JH, Zoncu R, Kim D, Sabatini DM. Defective regulation of autophagy upon leucine deprivation reveals a targetable liability of human melanoma cells in vitro and in vivo. Cancer Cell. 2011; 19(5):613–28. [PubMed: 21575862]
17. Creighton CJ, Li X, Landis M, Dixon JM, Neumeister VM, Sjolund A, et al. Residual breast cancers after conventional therapy display mesenchymal as well as tumor-initiating features. Proc Natl Acad Sci U S A. 2009; 106(33):13820–5. [PubMed: 19666588]
18. Shen C, Kaelin WG Jr. The VHL/HIF axis in clear cell renal carcinoma. Semin Cancer Biol. 2013; 23(1):18–25. [PubMed: 22705278]
19. Tang X, Keenan MM, Wu J, Lin CA, Dubois L, Thompson JW, et al. Comprehensive profiling of amino Acid response uncovers unique methionine-deprived response dependent on intact creatine biosynthesis. PLoS genetics. 2015; 11(4):e1005158. [PubMed: 25849282]
20. Murphy JM, Silke J. Ars Moriendi; the art of dying well - new insights into the molecular pathways of necroptotic cell death. EMBO Rep. 2014; 15(2):155–64. [PubMed: 24469330]
21. Sun L, Wang H, Wang Z, He S, Chen S, Liao D, et al. Mixed lineage kinase domain-like protein mediates necrosis signaling downstream of RIP3 kinase. Cell. 2012; 148(1-2):213–27. [PubMed: 22265413]
22. Chen X, Li W, Ren J, Huang D, He WT, Song Y, et al. Translocation of mixed lineage kinase domain-like protein to plasma membrane leads to necrotic cell death. Cell Res. 2014; 24(1):105–21. [PubMed: 24366341]
23. Cai Z, Jitkaew S, Zhao J, Chiang HC, Choksi S, Liu J, et al. Plasma membrane translocation of trimerized MLKL protein is required for TNF-induced necroptosis. Nature cell biology. 2014; 16(1):55–65. [PubMed: 24316671]

24. Tang X, Lucas JE, Chen JL, LaMonte G, Wu J, Wang MC, et al. Functional interaction between responses to lactic acidosis and hypoxia regulates genomic transcriptional outputs. Cancer research. 2012; 72(2):491–502. [PubMed: 22135092]
25. Galban S, Fan J, Martindale JL, Cheadle C, Hoffman B, Woods MP, et al. von Hippel-Lindau protein-mediated repression of tumor necrosis factor alpha translation revealed through use of cDNA arrays. Mol Cell Biol. 2003; 23(7):2316–28. [PubMed: 12640117]
26. Chen G, Goeddel DV. TNF-R1 signaling: a beautiful pathway. Science. 2002; 296(5573):1634–5. [PubMed: 12040173]
27. Wang CY, Mayo MW, Baldwin AS Jr. TNF- and cancer therapy-induced apoptosis: potentiation by inhibition of NF-kappaB. Science. 1996; 274(5288):784–7. [PubMed: 8864119]
28. Dillon CP, Weinlich R, Rodriguez DA, Cripps JG, Quarato G, Gurung P, et al. RIPK1 blocks early postnatal lethality mediated by caspase-8 and RIPK3. Cell. 2014; 157(5):1189–202. [PubMed: 24813850]
29. Oda E, Ohki R, Murasawa H, Nemoto J, Shibue T, Yamashita T, et al. Noxa, a BH3-only member of the Bcl-2 family and candidate mediator of p53-induced apoptosis. Science. 2000; 288(5468): 1053–8. [PubMed: 10807576]
30. Torres M, Forman HJ. Redox signaling and the MAP kinase pathways. Biofactors. 2003; 17(1-4): 287–96. [PubMed: 12897450]
31. Abram CL, Courtneidge SA. Src family tyrosine kinases and growth factor signaling. Experimental cell research. 2000; 254(1):1–13. [PubMed: 10623460]
32. Wang Z, Jiang H, Chen S, Du F, Wang X. The mitochondrial phosphatase PGAM5 functions at the convergence point of multiple necrotic death pathways. Cell. 2012; 148(1-2):228–43. [PubMed: 22265414]
33. Ploner C, Kofler R, Villunger A. Noxa: at the tip of the balance between life and death. Oncogene. 2008; 27(Suppl 1):S84–92. [PubMed: 19641509]
34. Murphy MP. How mitochondria produce reactive oxygen species. Biochem J. 2009; 417(1):1–13. [PubMed: 19061483]
35. Kim H, Koo S, Ahn B-H, Park O, Park D, Seo D, et al. NecroX as a novel class of mitochondrial reactive oxygen species and ONOO–scavenger. Archives of Pharmacal Research. 2010; 33(11): 1813–23. [PubMed: 21116785]
36. Gatza ML, Lucas JE, Barry WT, Kim JW, Wang Q, Crawford MD, et al. A pathway-based classification of human breast cancer. Proc Natl Acad Sci U S A. 2010; 107(15):6994–9. [PubMed: 20335537]
37. Pena-Llopis S, Vega-Rubin-de-Celis S, Liao A, Leng N, Pavia-Jimenez A, Wang S, et al. BAP1 loss defines a new class of renal cell carcinoma. Nat Genet. 2012; 44(7):751–9. [PubMed: 22683710]
38. Yagoda N, von Rechenberg M, Zaganjor E, Bauer AJ, Yang WS, Fridman DJ, et al. RAS-RAF-MEK-dependent oxidative cell death involving voltage-dependent anion channels. Nature. 2007; 447(7146):864–8. [PubMed: 17568748]
39. Dixon SJ, Lemberg KM, Lamprecht MR, Skouta R, Zaitsev EM, Gleason CE, et al. Ferroptosis: an iron-dependent form of nonapoptotic cell death. Cell. 2012; 149(5):1060–72. [PubMed: 22632970]
40. Kulbe H, Thompson R, Wilson JL, Robinson S, Hagemann T, Fatah R, et al. The inflammatory cytokine tumor necrosis factor-alpha generates an autocrine tumor-promoting network in epithelial ovarian cancer cells. Cancer research. 2007; 67(2):585–92. [PubMed: 17234767]
41. Wu Y, Zhou BP. TNF-alpha/NF-kappaB/Snail pathway in cancer cell migration and invasion. Br J Cancer. 2010; 102(4):639–44. [PubMed: 20087353]
42. Yang WS, SriRamaratnam R, Welsch ME, Shimada K, Skouta R, Viswanathan VS, et al. Regulation of ferroptotic cancer cell death by GPX4. Cell. 2014; 156(1-2):317–31. [PubMed: 24439385]
43. Motzer RJ, Hutson TE, Cella D, Reeves J, Hawkins R, Guo J, et al. Pazopanib versus sunitinib in metastatic renal-cell carcinoma. N Engl J Med. 2013; 369(8):722–31. [PubMed: 23964934]
44. Foulkes WD, Smith IE, Reis-Filho JS. Triple-negative breast cancer. N Engl J Med. 2010; 363(20): 1938–48. [PubMed: 21067385]

45. Ishimoto T, Nagano O, Yae T, Tamada M, Motohara T, Oshima H, et al. CD44 variant regulates redox status in cancer cells by stabilizing the xCT subunit of system xc(−) and thereby promotes tumor growth. Cancer Cell. 2011; 19(3):387–400. [PubMed: 21397861]

46. Yoshikawa M, Tsuchihashi K, Ishimoto T, Yae T, Motohara T, Sugihara E, et al. xCT inhibition depletes CD44v-expressing tumor cells that are resistant to EGFR-targeted therapy in head and neck squamous cell carcinoma. Cancer research. 2013; 73(6):1855–66. [PubMed: 23319806]

47. Xin H, Zhang C, Herrmann A, Du Y, Figlin R, Yu H. Sunitinib inhibition of Stat3 induces renal cell carcinoma tumor cell apoptosis and reduces immunosuppressive cells. Cancer research. 2009; 69(6):2506–13. [PubMed: 19244102]

48. Oya M, Ohtsubo M, Takayanagi A, Tachibana M, Shimizu N, Murai M. Constitutive activation of nuclear factor-kappaB prevents TRAIL-induced apoptosis in renal cancer cells. Oncogene. 2001; 20(29):3888–96. [PubMed: 11439352]

49. Godwin AK, Meister A, O'Dwyer PJ, Huang CS, Hamilton TC, Anderson ME. High resistance to cisplatin in human ovarian cancer cell lines is associated with marked increase of glutathione synthesis. Proc Natl Acad Sci U S A. 1992; 89(7):3070–4. [PubMed: 1348364]

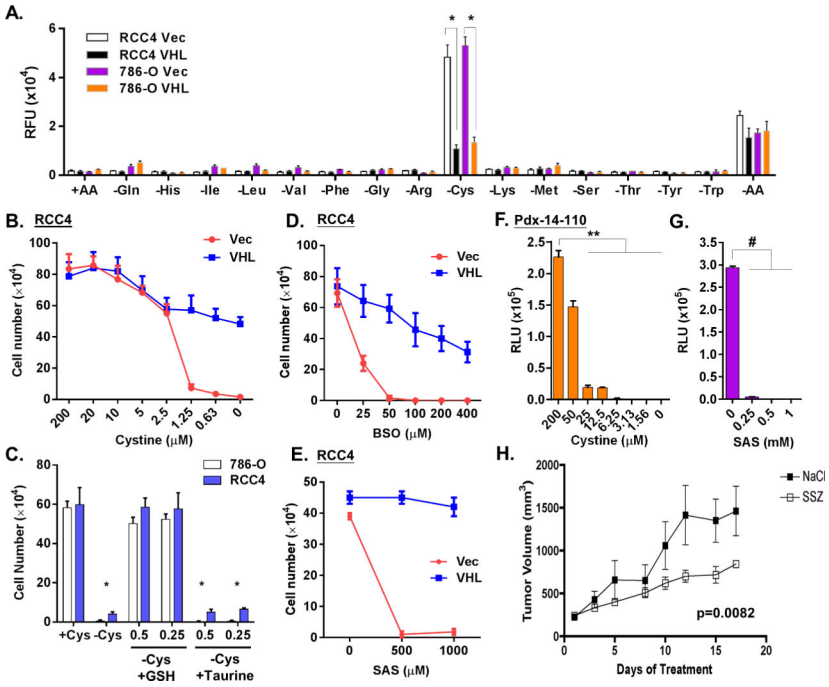

Figure 1. VHL renders renal cancer cell resistant to cystine-deprived cell death

(A). Cell cytotoxicity was determined by protease release of isogenic pairs of RCC4 and 786-O cells expressing either vector (Vec) or VHL (VHL) 24 hrs after the deprivation of indicated amino acid (n=3, $p<0.001$).

(B). Survival of RCC4 Vec and VHL cells after exposure to different levels of cystine (n=3, $p<0.01$).

(C). Survival of RCC4 or 786-O cells under cystine deprivation with or without the addition of GSH or taurine (n=3, $p<0.01$).

(D, E). Survival of RCC4 Vec and VHL cells after 72 hours treatment with buthionine sulfoximine (BSO, (D)) or sulfasalazine (SAS, (E)).

(F, G). Relative ATP levels in the patient-derived primary ccRCC cells after 3 days treatment with different doses of cystine (F) and SAS (G).

(H). The 786-O were injected subcutaneously to establish tumors until 250 mm^3 before starting treatments. The volume of 786-O tumor xenografts was measured for 17 days during the treatment with saline, or SAS (250 mg/kg). Data are presented for five animals per group ($p=0.0082$).

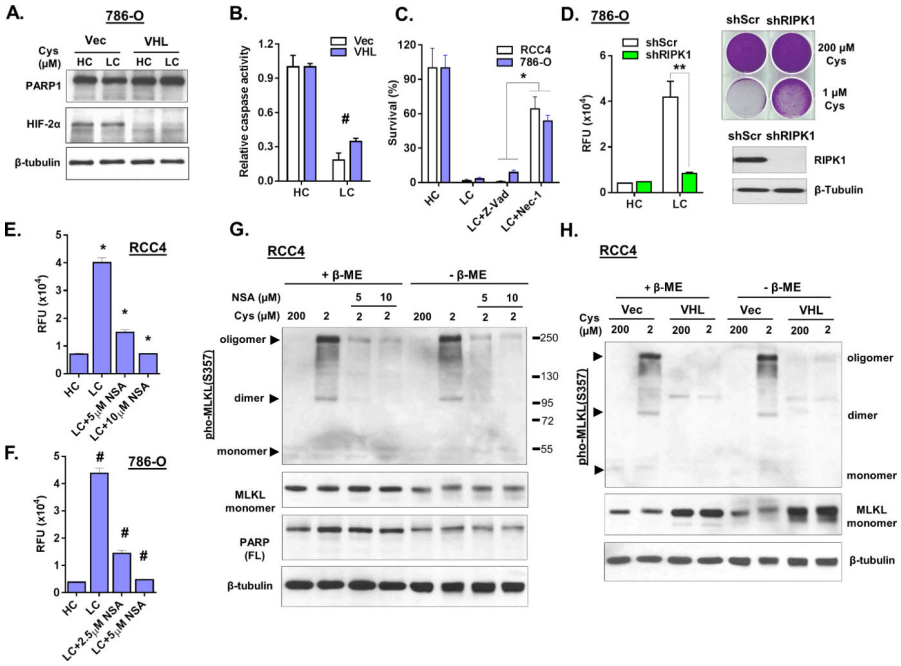

Figure 2. Cystine deprivation induces programmed necrosis in VHL-deficient RCC cells

(A, B). Analysis of PARP1, HIF-2α and β-tubulin protein (A) and relative caspase activity (B) in 786-O Vec and VHL cells after exposure to high (200 μM, HC) or low (1 μM, LC) cystine for 18 hours (n=3, $p < 0.05$).

(C). Survival of RCC4 and 786-O cells (n=4, $p<0.01$) in HC or LC media after 24 hours co-treated with the pan-caspase inhibitor (Z-Vad, 20 μM) or the necrosis inhibitor necrostatin-1 (Nec-1, 10 μM).

(D). Cell cytotoxicity (protease release) and viability (crystal violet staining) of 786-O scramble (shScr) and shRIPK1 cells after cystine deprivation. Immunoblotting of RIPK1 indicated the knockdown efficiency.

(E, F). Cell cytotoxicity of RCC4 (E) and 786-O (F) cells under LC media when treated with necrosulfonamide (NSA) for 24 hours (n=4, $p<0.005$).

(G). Analysis of MLKL, PARP1, and β-tubulin protein in RCC4 cells under indicated cystine levels when treated with indicated concentrations of NSA inhibitor for 16 hours. Protein samples were prepared in reducing (+ β-ME) or non-reducing condition (− β-ME).

(H). Analysis of MLKL protein in RCC4 Vec and VHL cells under indicated cystine levels for 16 hours and the samples were prepared as (G).

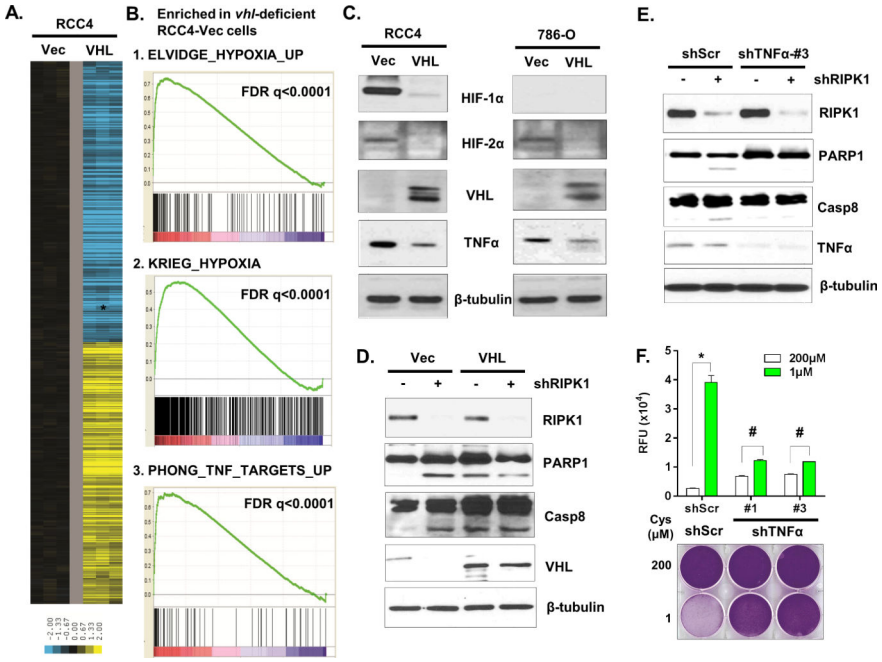

Figure 3. VHL prevents cystine-deprived necrosis by suppressing TNFα signaling

(A). Heatmap of selected genes whose expression was significantly altered by VHL restoration in RCC4 cells.

(B). GSEA analysis showed the enrichment of hypoxia and TNFα pathways in *VHL*-deficient RCC4.

(C). Analysis of HIF-1α, HIF-2α, TNFα, and VHL protein in RCC4 and 786-O cells infected with empty vector (Vec) or VHL (VHL).

(D, E). Analysis of PARP1 and caspase-8 (Casp8) cleavage in RCC4 Vec and VHL cells (D) or in RCC4 shScr and shTNFα cells (E) infected with shRIPK1 or control virus at day 5.

(F). Cell cytotoxicity and viability of 786-O scrambled (shScr) or two shTNFα cells after 24 hours of exposure to 200 or 1 μM of cystine (n=4; *, $p<0.01$; #, $p>0.05$).

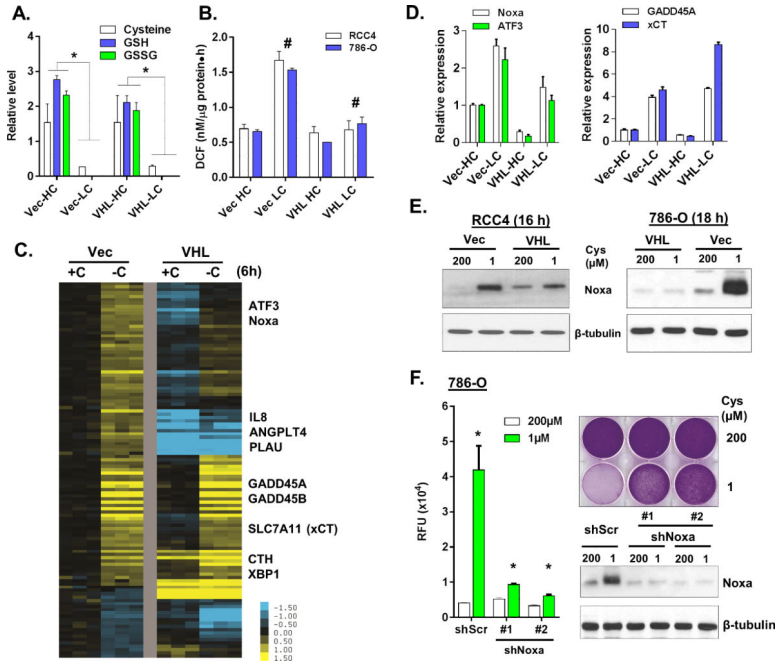

Figure 4. Metabolomic and transcriptional response to cystine deprivation

(A, B). Relative levels of cysteine, GSH and GSSG (A) as well as ROS (DCF, B) in 786-O Vec or VHL cells exposed to high (HC, 200 μM) or low cystine (LC, 1 μM) for 18 hours (n=3, $p<0.05$).

(C, D). Heatmap view (C) and RT-PCR (D) validated of indicated selected significantly altered genes expression in VHL-null and VHL-restored RCC4 after 6 hours cystine deprivation.

(E). Analysis of Noxa protein in Vec and VHL restored cells exposure high or low cystine.

(F). The cytotoxicity and viability of 786-O shScr and two shNoxa cells under indicated cystine concentrations for 24 hrs with representative Noxa protein expression (n=3, $p<0.001$).

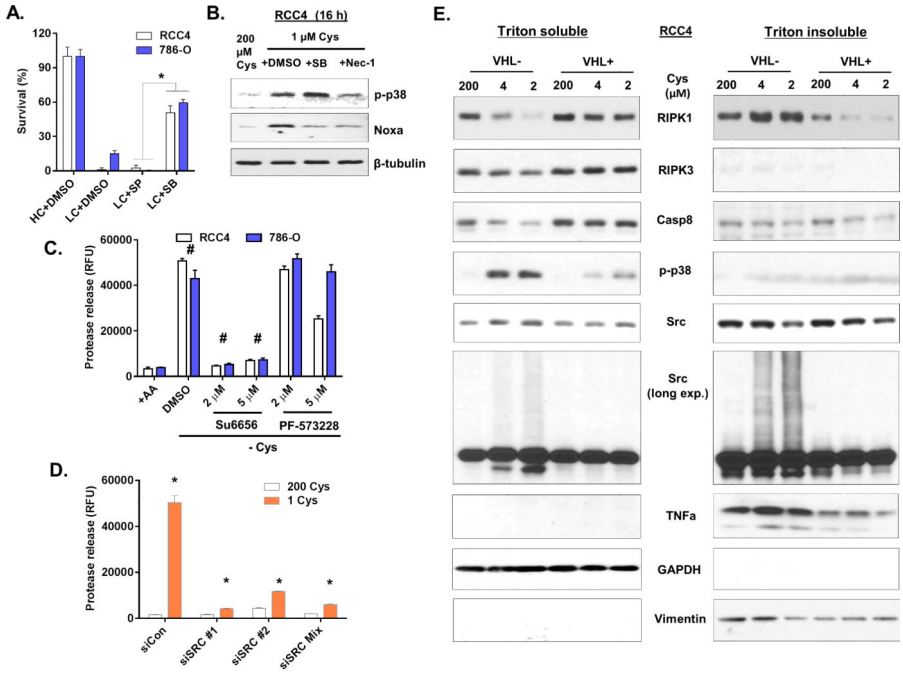

Figure 5. The activation of Src and p38 kinases is required for cystine-deprived necrosis

(A). Relative survival of RCC4 and 786-O cells under high (HC, 200 μM) or low cystine (LC, 1 μM) treated with inhibitors of p38 (SB) or JNK (SP) (n=3, $p<0.005$).

(B). Immunoblotting of phosphorylated p38 (p-p38) and Noxa protein expression in RCC4 cells under indicated levels of cystine for 16 hours with or without p38 inhibitor (SB) or Necrostatin-1 (Nec-1).

(C). Cell cytotoxicity of RCC4 and 786-O cells under cystine deprivation with Src inhibitor (Su6656) and FAK inhibitor (PF-573228) for 24 hours (n=4, $p<0.001$).

(D) Cell cytotoxicity of 786-O cells transfected with siCon, individual or pooled siSrc under indicated cystine levels for 24 hours (n=3, $p<0.001$).

(E). Western blots analysis of indicated proteins in the fraction of cytosol (Triton soluble) and membrane (1%SDS, Triton insoluble) fraction of RCC4 Vec and VHL cells under indicated cystine levels for 18 hours.

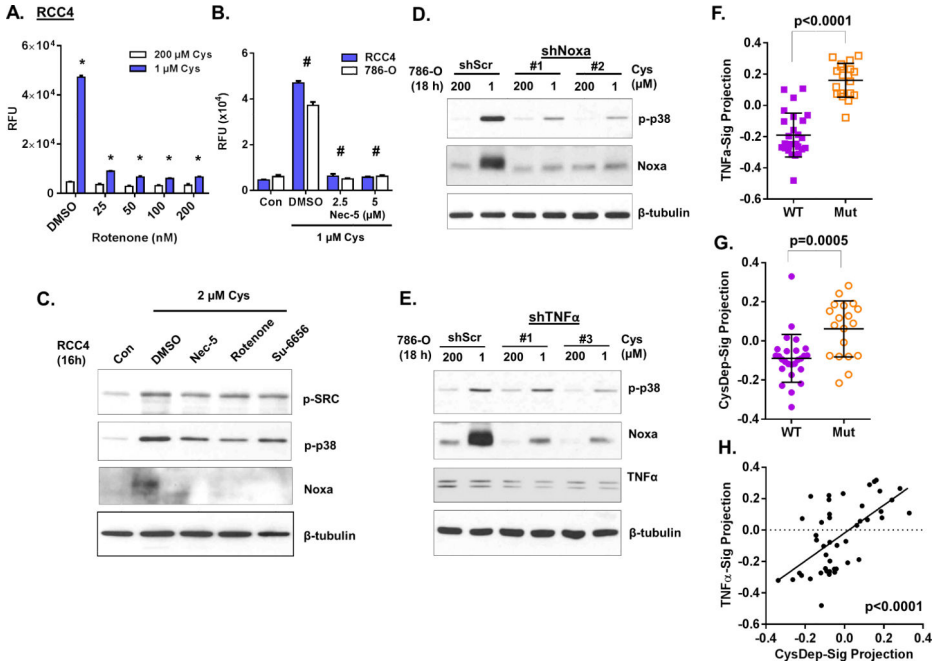

Figure 6. Mutual amplification between the Src-p38-Noxa and TNFα-RIP1/3-MLKL pathways

(A, B). Cell cytotoxicity of indicated cells after 24 hours of cystine deprivation in the presence or absence of rotenone (A) or Necrox-5 (Nec-5, B) at indicated concentrations (n=4, p<0.005).

(C). Western blots analysis of p-Src, p-p38 and Noxa protein after 16 hours of cystine deprivation in the presence different inhibitors.

(D, E). Immunoblotting of pho-p38 and Noxa protein expression in 786-O shScr and shNoxa (D) or shTNFα (E) cells after 18 hours cystine deprivation.

(F, G, H). The activities of CysDep (A) or TNFα (F) or CysDep (G) gene signature and their correlation (H) in a dataset of normal tissue and ccRCC with *VHL* gene status (WT or Mut).

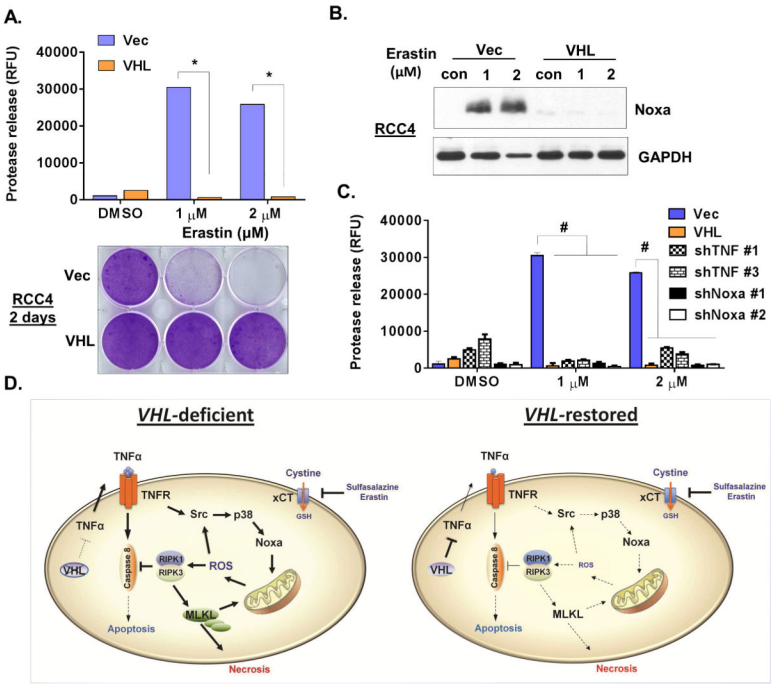

Figure 7. Low doses of erastin share a similar mechanism as cystine deprivation to trigger programmed necrosis in ccRCC

(A). Cell cytotoxicity (24 hours, n=4, $p<0.001$) and crystal violet staining (2 days) of RCC4 Vec and VHL cells treated with indicated concentrations of erastin.

(B). Western blots analysis of Noxa protein induction in RCC4 Vec and VHL cells treated with indicated concentrations of erastin.

(C). Cell cytotoxicity (24 hours, n=3, $p<0.05$) of 786-O Vec, VHL and different shRNA sub-lines cells treated with indicated concentrations of erastin.

(D). Model of the distinct signaling components triggered by cystine deprivation in *VHL*-deficient and *VHL*-restored ccRCC.